Available online at www.sciencedirect.com
SCIENCE DIRECT
Polymer 46 (2005) 11610–11623
polymer
www.elsevier.com/locate/polymer

Adhesion of CPO onto high modulus TPO: Lap-shear tests in conjunction with microscopy studies of the fracture surface structure

Zhihui Yin [a], Yuechun Ma [a], Warner Chen [a], Neil Coombs [a], Mitchell A. Winnik *,[a], Rose A. Ryntz [b], Philip V. Yaneff [c]

[a] *Department of Chemistry, University of Toronto, 80 St George Street, Toronto, Ont., Canada M5S 3H6*
[b] *Visteon Automotive Systems, Dearborn, MI 58121, USA*
[c] *E.I. Dupont Canada, 408 Fairall Street, Ajax, Ont., Canada L1S 1R6*

Received 19 July 2005; received in revised form 23 September 2005; accepted 26 September 2005
Available online 25 October 2005

Abstract

A lap-shear test was employed to investigate the failure mechanism of a chlorinated polyolefin (CPO) coating on a high-modulus thermoplastic olefin (TPO) substrate fabricated as a blend of a highly crystalline Ziegler-Natta isotactic polypropylene (iPP) and a crystalline metallocene poly(ethylene–butene) (9 wt% butene, EB9) impact modifier. The CPO was a chlorinated polypropylene containing 20 wt% Cl. The results showed that the fracture strength increased with increasing EB9 content in TPO blends. They also showed that the presence of xylene vapor during the bake step improved the adhesion between CPO and iPP itself (by 40%), but had a much smaller effect for the TPOs. Optical and transmission electronic microscopy images revealed a well-defined skin layer approximately 230 μm thick at the mold surface of the injection molded substrates. For the 25 wt% EB9 blend (TPO_{25}), this skin layer consists of thin fibers of EB trapped in a transcrystalline iPP matrix, with crystalline lamellae propagating from the matrix across the EB9 domains. Laser scanning confocal fluorescence microscopy (LCFM) and scanning electron microscopy images of iPP/CPO/iPP samples indicate that failure occurred close to the interface between the CPO and the iPP substrate, and, during fracture, the CPO layer maintained its original thickness. For the TPO/CPO/TPO sandwich samples, the fracture surfaces themselves were much rougher than that between CPO and iPP. Substantial deformation of the CPO layer was seen in the fractured samples, and failure was due primarily to cohesive fracture of the CPO in the region adjacent to the TPO substrate. From the perspective of newly introduced environmental regulations restricting aromatic hydrocarbons in automotive coatings, the most important result was the strong adhesion between CPO and TPO_{25}, with little difference between the samples exposed to xylene vapor and those not exposed to xylene.

Keywords: TPO/CPO adhesion; Lap-shear test; Laser confocal fluorescence microscopy scanning electron microscopy

1. Introduction

This paper reports experiments that investigate the adhesion between a chlorinated polyolefin (CPO) and injection-molded isotactic polypropylene (iPP) blends. The particular polypropylene blends of interest here are intended for use as lightweight components for automotive applications. These blends differ in two ways from many similar types of 'thermoplastic polyolefin' (TPO) blends that have been examined in the past. First, the iPP itself is a high modulus, relatively high molar mass Ziegler-Natta product with a very small amorphous component. In addition, the impact modifier is a rather crystalline metallocene copolymer of ethylene and butene (EB). Many plastic automotive parts such as bumpers and fascia are fabricated from TPO. These parts are normally painted to match the color of the rest of the vehicle. Coating failure on thermoplastic polyolefin substrates has been a problem confronting the automotive industry for many years. The poor paintability of TPO substrates results from its low surface energy, as well as the lack of active groups, and the chemical inertness of the main TPO components. For high modulus TPO containing a semicrystalline impact modifier, achieving good paint adhesion is an even bigger challenge than for traditional TPOs.

For proper paint adhesion to TPO, additional surface treatments are required. These include plasma or flame treatment or corona discharge to oxidize the surface to introduce polar groups [1]. Another major strategy for surface preparation is the application of a thin layer of adhesion

* Corresponding author. Tel.: +1 416 978 6495; fax: +1 416 978 0541.
E-mail address: mwinnik@chem.utoronto.ca (M.A. Winnik).

0032-3861/$ - see front matter © 2005 Elsevier Ltd. All rights reserved.
doi:10.1016/j.polymer.2005.09.078

promoter (AP) to the TPO surface to enhance the coating adhesion to TPO. Most adhesion promoters are formulations containing chlorinated polyolefin (CPO) as the critical adhesive binder. The adhesion promoter is regarded as a coupling agent in the painted TPO system, and TPOs of different composition can require different CPOs for optimum performance. Although CPO has been used as adhesion promoter in the automotive industry for many years, knowledge about how CPO promotes coating adhesion to TPO is limited, and obtaining reproducible results is challenging because of the complexity and variability of the underlying TPO substrate [2].

To appreciate some of the complexities, consider first that while paint will adhere to CPO-primed injection-molded TPO, the adhesion is substantially poorer if the TPO of the same composition is compression molded [3]. One concludes that the processing conditions must affect the surface morphology of the TPO blend in a way that is essential for obtaining good paint adhesion. For polymer blends like TPO, injection molded components are formed under non-equilibrium conditions in which shear forces associated with flow fields and temperature gradients associated with the mold surface affect the overall morphology in ways that are not well understood. These processing conditions can affect the fraction of the impact modifier component at the TPO surface as well as the nature of the crystalline iPP domains near or at the surface. In one study, Ryntz and Ramamurthy [4] found, using X-ray microfocus fluoroscopy, a thin skin layer of higher crystallinity at the surface of an injection molded iPP/EPR (TPO) blend (EPR is ethylene–propylene rubber), which they attributed to a transcrystalline iPP layer. Beneath this layer was a thick region containing large iPP spherulite crystals followed by a layer rich in EPR. EPR domains near the surface tended to be elliptical, with the long axis of the domains following the flow direction of the TPO melt. Beyond these global aspects of the morphology of this particular blend, the authors comment that TPO has a high spatial heterogeneity in all dimensions that is difficult to characterize [5].

In a later publication, Mirabella et al. [6] examined cryomicrotomed sections of painted CPO-coated injection molded TPO plaques, using a combination of transmission electron microscopy (TEM), atomic force microscopy (AFM), and scanning transmission X-ray microscopy (STXM). They found no indication of a transcrystalline iPP layer at the TPO/CPO interface, but good evidence for the presence of EPR droplets in the iPP matrix in the near-surface region of this component and in contact with the CPO. While these results may appear to be in contradiction, the processing conditions for the injection molding also appear to be different. From analysis of the STXM profiles, the authors estimated an interface width on the order of 350 nm between the CPO and TPO components. This is much wider than the value of 11 nm that they estimated from thermodynamic considerations.

More recently, Tang and Martin [7] carried out interfacial deformation and delamination tests, as well as a detailed examination by optical and electron microscopy of painted commercial TPO plaques. They saw clear evidence for an iPP-rich layer at the TPO surface, ranging in thickness from a few hundred nanometers to several micrometers. Their TEM images (e.g. Fig. 3 in Ref. [7]) show a well-elongated fibrous morphology of the rubber components in the iPP matrix and just below the iPP-rich layer. Baking the sample at 120 °C for 45 min led to a significant amount of swelling of the rubber phase in the near-surface area, as well as diffusion of the rubber into the iPP-rich layer.

All studies of CPO-coated TPO indicate that the presence of the impact modifier improves adhesion between the CPO and the polypropylene substrate. For example, Tomasetti et al. [8] reported that the adhesion of the CPO onto the blends of iPP and EPR was much better than its adhesion to the pure iPP component. These observations led to the idea that there is greater thermodynamic miscibility between the impact modifier and CPO than for iPP, i.e. there is a smaller Flory–Huggins χ parameter for CPO/EP or EB than for CPO/iPP. Ellis [9] tried to test this idea by using a group-additivity approach to estimate values of χ for mixtures of various chlorinated PP compositions with PP, PE, and various EP copolymers. Except for a narrow composition range of EP and a relatively narrow blend composition, chlorinated PP was predicted to be more miscible with PP than with the other polyolefins. For the case of EP containing 35 wt% E and a chlorinated PP with 21 wt% Cl, the estimated interaction parameter χ was lower (0.0058) for this EP than for PP (0.0063). This analysis ignores the contribution of the polar succinic anhydride groups (or carboxylic acid groups upon hydrolysis) that are part of the CPO structure, and the influence of temperature associated with the annealing step used to promote adhesion. The widths of the interface predicted by these values of χ are much narrower than that found by Mirabella [6] and by Tang and Martin [7].

In many of the older studies in the literature, the impact modifier was an ethylene–propylene copolymer with little if any crystalline content. Most experiments were carried out on painted TPO plaques prepared from fully formulated TPO blends containing fillers and additives. Often the composition of the basecoat and clearcoat are not specified. The composition of the TPO and adhesion promoter are not described in detail, and the molecular details of these components are either unknown to the experimenters because they are working on commercial samples, or are not reported. Such studies provide important information for understanding the global behavior of plastic parts produced for commercial applications, but they leave unanswered many important fundamental scientific issues about the factors that affect morphology, interface structure, and adhesion for adhesion-promoter-coated TPO. For this type of knowledge, it is advantageous to take a more reductionist approach, examining interactions between individual components with known composition and molar mass, controlling as much as possible the processing conditions.

In a recent publication [10], we described experiments that can be considered as an extreme example of this approach. We prepared traditional blends of a small amount of dye-labeled CPO with a 75/25 w/w mixture of iPP and EB using the same

CPO, iPP and EB9 samples examined in this paper. Laser scanning confocal fluorescence microscopy (LCFM) experiments showed that in these quiescent blends prepared above the melting temperature of iPP, that the CPO engulfed droplets of EB9 in the iPP matrix. This result provides unambiguous evidence that there is a much smaller interfacial energy between CPO and EB9 than between CPO and iPP. In addition, we reported that close inspection of the boundary region between the CPO and EB9 indicated that there was a relatively diffuse interface between these two components.

Here we describe adhesion measurements based upon lap-shear tests for samples in which a layer of CPO approximately 10 μm thick is used to join two substrates. The substrates are injection-molded plaques consisting of either pure iPP, or model TPO formulations containing 12 wt% EB9 (TPO_{12}) or 25 wt% EB9 (TPO_{25}). The CPO is covalently labeled with a small amount of a fluorescent dye, and we use a combination of scanning electron microscopy (SEM) and laser scanning confocal fluorescence microscopy (LCFM) to examine the morphology of the fracture surfaces. We also provide high-resolution transmission electron microscopy TEM images of cryo-sectioned samples that that help us understand the near-surface morphology of the injection-molded TPO_{25} sample.

2. Experimental

2.1. Materials

Isotactic polypropylene (Escorene 1042, Ziegler-Natta catalyst), poly(ethylene–butene) (Exact 3125, with 9 wt% butene, metallocene catalyst) copolymer used in this study are from ExxonMobil. According to Ref. [11], these polymers are characterized by $M_n = 67{,}070$ g/mol (PDI = 3.51) for iPP and $M_n = 45{,}562$ g/mol (PDI = 1.96) for EB9. Chlorinated polypropylene (CPO Superchlon 872S) with 20 wt% chlorine content was provided by Nippon Paper Chemicals Co. Ltd. By gel permeation chromatography (GPC, polystyrene standards), we determined the molecular weight of this CPO sample to be $M_w = 92{,}000$, $M_n = 41{,}000$. The anhydride content was determined by titration and found to be 0.19 mmol/g polymer [10]. As described in a previous publication [10], a sample of this polymer was functionalized with a benzothioxanthene (HY) fluorescent dye to yield a dye-labeled polymer (CPO-HY) with a maximum absorbance in the UV–vis spectrum of $\lambda_{max} = 456$ nm, and a dye content of 0.06 mmol/g. In all experiments reported here, the CPO sample contained 5 wt% of this dye-labeled polymer.

2.2. iPP and TPO blend preparation

The TPO blends were prepared by premixing polypropylene with different amounts of EB9. The mixtures were then run through a twin-screw mini-extruder (15 cm^3 capacity, DSM, The Netherlands) and extruded through a single strand die. The extruder was pre-heated to the following conditions for all of the TPO blends and iPP materials: 190 °C for the near feeder block, 215 °C for the middle block, and 230 °C for the near die part. The screw was run at a constant speed of 100 rpm for all of the formulations. Each blend was molded into a rectangular plaque (60 × 12.6 × 2.0 mm) through a 2.0 mm wide pin gate using a DSM microinjection-molding machine (3.5 cm^3) at 70 psi injection pressure with a mould temperature of 43 °C.

2.3. Lap-joint test

One surface of each of the iPP or TPO plaques was spin-coated (1000 rpm) with a solution (10 wt%) of CPO in tetrahydrofuran (THF). We use THF as the solvent to minimize solvent penetration into the plaques. The thickness of the dry CPO layer was about 5 μm. After drying for 24 h at room temperature, some of the plaques were baked at 120 °C for 20 min to promote adhesion of CPO to the iPP or TPO substrates. Other samples were heated at 120 °C in the presence of xylene vapor. The treatment was performed in a sealed glass container. Bilayer samples (e.g. CPO/iPP and CPO/TPO) were placed on a support in the middle of the container that contained liquid xylene at the bottom. The container was placed in an oven at 120 °C for 20 min. After the bake step, sandwich-like three-layer samples (iPP/CPO/iPP or TPO/CPO/TPO, or iPP/CPO/TPO) were prepared from pairs of CPO coated plates. To prepare an individual sample, a pair of CPO coated substrates was placed in the appropriate lap-shear geometry (Fig. 1) with the two CPO layers in contact, and then the sandwich sample was heated at 100 °C for 5 min in a Carver Press under gentle pressure to make the central CPO layers join well for the lap-shear test. The contact dimensions were

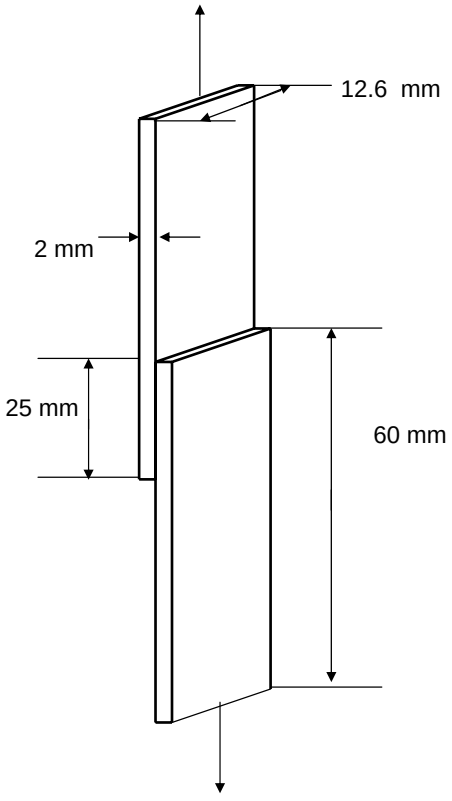

Fig. 1. Lap shear joint geometry used in this work.

12.6 mm wide and 25 mm long, and this part was always taken from the near-gate part of the injection-molded iPP or TPO plates. The bonded joints were subjected to shear fracture in tension on an Instron 5545 tester at room temperature. Force–displacement curves were recorded at a crosshead speed of 5 mm/min. At least five specimens of each sample were tested.

2.4. Scanning (SEM) and transmission (TEM) electron microscope

A Hitachi S-5200 scanning electron microscope, operated at 0.5 kV, was used to characterize the fracture surface morphology of the lap-joint test samples. At this low accelerating voltage, there was no need to treat the sample surfaces. TEM measurements were carried out at 200 kV using a Hitachi HD-2000 instrument. For the samples examined here, we obtained much better contrast in the dark-field mode, and all TEM images shown below are dark-field images. Seventy nanometers sections of TPO and CPO-coated TPO were obtained by cryogenically microtoming samples on a Leica (EM FCS) microtome with a MC 1029 35° diamond knife at −140 °C. Sections were stained by exposure to RuO_4 vapor for 30 min in a closed chamber.

2.5. Differential scanning calorimetry (DSC)

A TA Q-100 DSC was used for calorimetric studies. Materials from the injection bar were heated from room temperature to 215 °C at a rate of 10 °C/min. The melting temperature was taken as the temperature corresponding to the peak in heat flow during the heating step. Enthalpies of crystallization and melting were obtained by integrating the heat flow curve to a flat baseline. Using the known heat of fusion of a perfect iPP (207 J/g) and PE (288 J/g) crystal [12], the weight fraction crystallinity was calculated as,

$$X_c = \frac{\Delta H_m}{f \Delta H_m^0} \quad (1)$$

where ΔH_m is the measured enthalpy of melting, ΔH_m^0 is the ideal enthalpy of melting a perfect crystal of polymer X, and f is the weight fraction of the polymer in the blend.

2.6. Laser scanning confocal fluorescence microscopy measurements

The fracture surface morphology of individual iPP/CPO/iPP and TPO/CPO/TPO sandwich samples was visualized using a Zeiss LSM 510 Laser scanning confocal fluorescence microscope (LCFM) system fitted with a water-immersion objective. The samples were excited with the 488 nm line of an argon laser line. The light emitted was collected in the range 510–550 nm through a band-pass filter. Optical slices ranging from 0.6 to 0.8 μm thick were obtained by setting the pinhole in the range of 65–100 μm. The instrument was operated in the frame scan mode to obtain top view images of the fracture surfaces. The XZ-direction multi-line scan mode was used to obtain cross-section-view images of the fracture surface of the lap-shear samples.

2.7. Optical microscopy measurements

Fifteen to twenty micrometers thick sections of injection molded iPP or TPO sample were obtained by cryogenically microtoming samples on a Leica (EM FCS) microtome using a glass knife at −60 °C. Optical microscopy analysis was performed under crossed polarizers at a magnification of 20X on an Olympus BX41 microscope.

3. Results and discussion

The protocol for the experiments reported here was designed to model aspects of the processing conditions used for the painting of plastic automotive parts. To overcome the poor adhesion of basecoat on the TPO surface itself, injection-molded TPO parts are often coated with CPO as an adhesion promoter. The CPO is applied as a solution in an organic solvent mixture that contains an aromatic solvent component. The function of the aromatic solvent is to help swell the substrate, ostensibly to promote diffusion of the CPO polymer chains into the polymers that comprise the TPO. Under some circumstances, the CPO-coated part is subjected to a pre-bake at 120 °C prior to being painted. In other circumstances, basecoat and clearcoat are applied wet-on-wet-on-wet over the CPO layer, and the three layer coating is baked at 120 °C. We note first, that this temperature is above the melting temperature (T_m) of the linear EB9 polymers used as the impact modifiers in our TPO sample, but well below the normal melting temperature (ca. 165 °C as shown in Table 1) of the iPP matrix. In addition, we note that in the three-layer wet coating, the TPO is exposed to a hot aromatic-containing solvent for a significant time. This solvent exposure is thought to enhance adhesion. We tested the influence of the aromatic component in the CPO coating solution by exposing the coated part to xylene vapor at 120 °C before fabricating the sandwich structures used for lap-shear testing.

Table 1
Composition and thermal data for iPP and TPOs

Sample	iPP (wt%)[a]	EB9 (wt%)[a]	T_m (°C)	ΔH (J/g) ($\Delta H/\Delta H^{0\%}$)[b]
iPP	100	–	165.2	90.64 (43.4%)
EB9	–	100	106.6	83.60 (29%)
TPO_{12}	88	12	iPP 165.5	79.98 (43.5%)
			PE 106.3	6.7 (19.4%)
TPO_{25}	75	25	iPP 165.5	65.98 (42%)
			PE 106.0	16.42 (22.8%)

All the samples were prepared by mini-extruder at 230 °C/100 rpm/5 min, and then injection molded at 230 °C/70 psi with a mold temperature of 43 °C.

[a] iPP, polypropylene (Exxon Escorene 1042); EB9, (Exxon Exact 3125, 9 wt% butene).

[b] From DSC measurements under N_2 for scans at 10 °C/min from 20 to 215 °C. The percent of crystallinity was calculated as ($\Delta H/\Delta H^0 \times 100$), where ΔH^0 is the known enthalpy of melting of perfect crystalline polypropylene ($\Delta H_{PP}^0 = 207$ J/g) and polyethylene ($\Delta H_{PE}^0 = 288$ J/g).

The samples were prepared by coating individual iPP or TPO substrates with CPO to form a layer very close to 5 μm thick. We employed tetrahydrofuran as a solvent for this coating because it is a poor solvent for both iPP and EB9. In this way we hoped that these coating conditions would not promote CPO penetration into the substrate. As explained in Section 2, these bilayer samples, after thorough drying, were annealed at 120 °C, either dry or exposed to xylene vapor. Then a three-layer sandwich was assembled in a lap-shear geometry by gently pressing the two CPO surfaces together at 100 °C. Thus, the CPO layer between the substrates has an initial thickness of ca. 10 μm.

In addition to measuring the lap-shear strength, we investigated the fracture surfaces by SEM and by LCFM. The LCFM experiments take advantage of the fact that a small fraction of the CPO component is covalently labeled with a fluorescent dye. The main advantage of using LCFM as a tool to study the surface structure of polymers, compared to SEM, is that LCFM can provide information simultaneously about the surface morphology and composition. It can also sample larger areas than SEM (several 100 μm) in a non-invasive manner. Of course it is limited in its resolution to features larger than 0.3–0.5 μm.

Fluorescence microscopy requires that the component to be monitored be labeled with a fluorescent dye. In the experiments reported here, we employed a CPO in which a portion of the sample had been reacted with an amino-functional benzothioxanthene dye. This dye-labeled CPO (CPO-HY) serves as a tracer for the CPO phase. The structure of this dye and that of a free-dye analogue, the commercial dye Hostasol Yellow 3G, are shown in Chart 1.

We begin by considering the initial sample morphology in the surface region of the sample. In Fig. 2, we show four images, three LCFM images in cross section of CPO coated TPO reflecting different stages and protocols in sample treatment, as well as a transmission electron microscopy (TEM) image of a CPO coated TPO. The LCFM images were obtained non-destructively using the XZ-scan technique. In this approach, the fluorescence intensity was collected along a single line, and at each successive scan, the focus was moved 1.0 μm in depth. The software built the fluorescent intensity profiles into images along the *xz* plane, where *x* is the lateral dimensions and *z* is the focal dimension. The dye-labeled CPO layer appears light gray in the gray-scale images shown here. From these images, one sees that the top surface is flat (on a micrometer scale) and that the CPO layer is uniform and almost exactly 5 μm thick. One can see what appears to be roughness at the CPO–TPO interface. In Fig. 2(a), for the sample prepared by spin coating from THF solution, this roughness appears as short spikes, only one pixel wide, and may be an artifact of the data acquisition technique. In the sample annealed for 20 min at 120 °C (Fig. 2(b)) and the film exposed to xylene vapor for 20 min at 120 °C, Fig. 2(c), there is a large scale waviness that may indicate changes in the interfacial region upon heat treatment. We anticipate reporting a more detailed investigation of the interface region, as studied by high resolution TEM, in the near future.

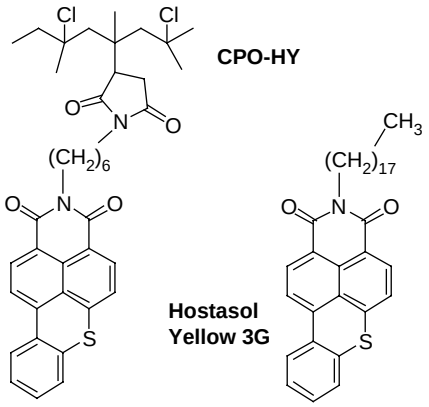

Chart 1.

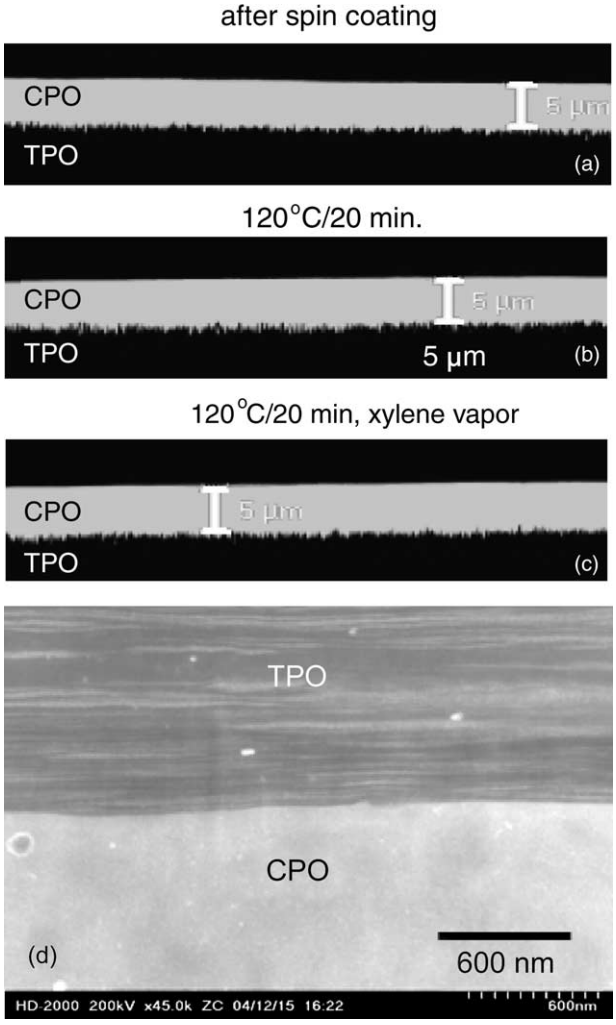

Fig. 2. Side view LCFM and TEM images of CPO coated TPO; (a) side view LCFM image of CPO/TPO_{25} after spin-coating; (b) side view LCFM image of CPO/TPO_{25} baked at 120 °C/20 min; (c) side view LCFM image of CPO/TPO_{25} baked at 120 °C/20 min/xylene vapor; (d) TEM image (dark-field) of the CPO/TPO_{25} after spin-coating (the sample was stained by RuO_4 vapor for 30 min).

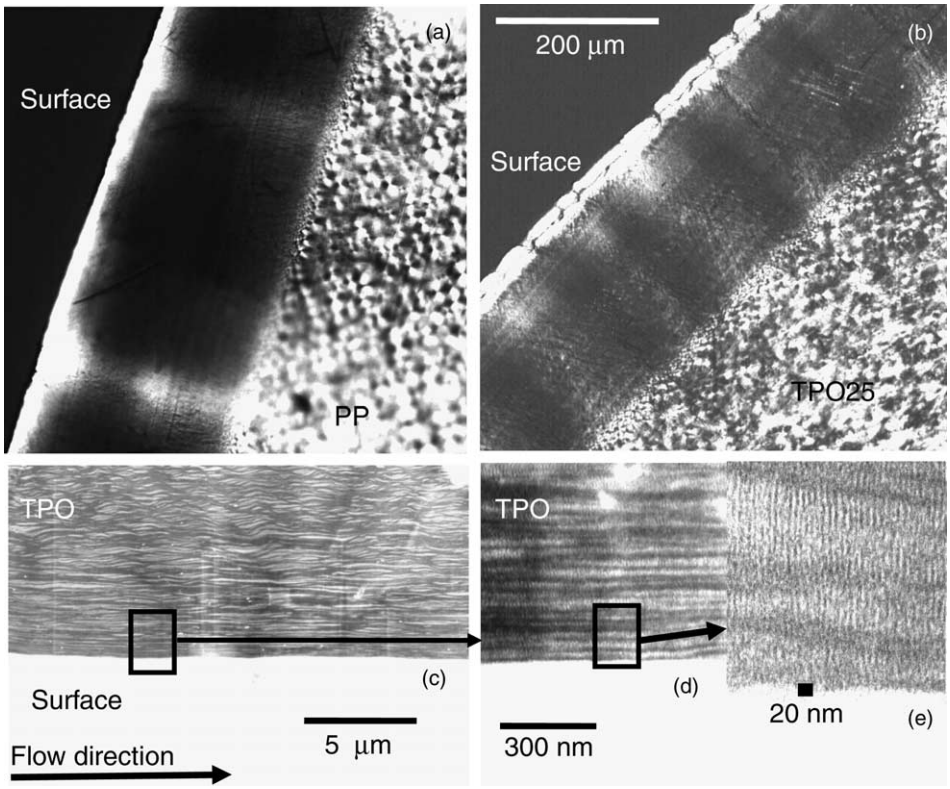

Fig. 3. Polarized microscopy images in the near-surface region of injection molded bars of (a) PP and (b) TPO_{25} cryo-sectioned parallel to the flow direction. (c)–(e): TEM images of a TPO_{25} sample cryo-sectioned parallel to the flow direction, at three increasing levels of magnification as indicated by the scale bars.

In Fig. 2(d), we present a near surface dark-field TEM image of a CPO coated TPO_{25} blend without thermal treatment. The sample was prepared by cryo-microtoming the CPO-coated TPO substrate after the THF coating solvent had completely evaporated. The section was cut parallel to the injection direction, and was stained with ruthenium tetroxide (RuO_4) vapor for 30 min at room temperature. RuO_4 stains the amorphous (primarily EB9) domains of the TPO. Untreated CPO is not stained by RuO_4 and is hard to distinguish from other white domains in a TEM image. RuO_4 is a powerful stain for the HY dye groups present in trace quantities in the CPO. Fortunately for us, this staining step imparts a light gray color in the dark-field image that provides very useful contrast between the CPO and the TPO components. Among the prominent features that one can see in the image is that the EB9 domains become highly stretched in the near-surface region as a consequence of the injection molding conditions used to prepare the substrates. We will have more to say about the TPO morphology in the near-surface region in the following paragraphs. One can also see that the CPO/TPO interface in this as-prepared sample is relatively sharp on a length scale of 100 nm.

A striking characteristic of injection-molded iPP is the presence of a skin layer consisting of a highly birefringent region very different from the spherulite crystals found in bulk. The skin layer is formed through shear-induced crystallization in the surface region of the mold. This effect has been noted by many research groups and studied in detail, particularly by Fujiyama [13] and by Kornfield [14]. As a test of our injection molding conditions, we examine polarized optical microscopy images of cryo-sectioned samples of iPP (Fig. 3(a)) and TPO_{25} (Fig. 3(b)). These sections were cut perpendicular to the flow direction from samples taken near the gate of the mold. One can see a ca. 230 µm thick skin layer on the top surface of both samples. We repeated these experiments for samples taken far from the gate (here 5.0 cm) and half-way along the sample. For iPP, we found, as is well known from the work of Fujiyama et al. [13], that the skin layer thickness of injection molded iPP samples decreased with increasing distance from the gate. The values we obtained are collected in Table 2. We note that the skin layer for TPO_{12} and for TPO_{25} show substantially less variation with distance from the gate than iPP itself. This result is consistent with that reported by Ryntz [15], who noted that the molding shear stress had little effect on skin layer thickness of a TPO blend when an elastomer with relatively high crystallinity was used, and the shear stress decreased with the distance from the gate position during injection the molding process.

What is more difficult to determine is the morphology of the impact modifier within the skin layer and adjacent to the mold surface for injection molded TPO. The RuO_4-stained TEM images reported by Tang and Martin [7] showed fiber-like rubber domains in the near-surface region of their painted TPO samples, but no information was available about the composition of the iPP-rich region at the TPO–CPO interface. Moffitt et al. [16] used LCFM measurements (with dye-labeled

Table 2
Skin layer thickness of PP and TPO blends

Sample	PP crystallinity (%)[a]	Skin layer thickness (μm)		
		Near gate	Center	Far from gate[b]
PP 1042	43.4	230	200	100
$TPO9_{12}$ (PP/EB9 88/12 wt%)	43.5	220	210	140
$TPO9_{25}$ (PP/EB9 75/25 wt%)	42	225	225	180

[a] See Table 1.
[b] Five centimeters from the gate.

EB) to study the morphology of a model TPO blend consisting of the same iPP sample employed here, but a more amorphous EB containing 28 wt% butane. Those samples were subjected to a laminar flow pulse at 153 °C, below the normal melting temperature of iPP. The shear induced crystallization of the iPP in the near surface region trapped the EB domains in the form of elongated fibers.

Here we obtain information about the near-surface morphology from the dark-field TEM images of the RuO_4 stained samples, obtained by cryo-sectioning along the flow direction. These images are shown at three levels of magnification in the lower part of Fig. 3. On the left-hand side, Fig. 3(c), one can observe striations in the flow direction, in which the dark domains in the dark-field image are due to the iPP matrix, and we attribute the lighter (stained) domains primarily to EB. The bottom of the image corresponds to the TPO/air-surface. It is clear that the EB domains are highly stretched in the flow direction, and at this level of magnification, the fibers are very thin. Upon close inspection of this image, one can see that the aspect ratio of the EB domains become smaller with increasing distance from the surface. In the adjacent image (Fig. 3(d)), one can see that the fibers of EB approach very close to the surface of the sample. In this image it appears that there is a thin (ca. 10–20 nm thick) layer of crystalline iPP at the surface. In previous studies of CPO-coated TPO fabricated with a much lower modulus TPO, the results were interpreted in terms of a layer of an amorphous atactic PP layer [17] or a PP rich layer [7] at the surface of the injection molded TPO. The iPP sample employed in these studies has a very low atactic content, and there is no indication of an amorphous polymer layer at the sample surface.

At the highest level of magnification (Fig. 3(e)) one can see lamellae extending perpendicular to the surface. Thus, we see that there is a pronounced trans-crystalline layer in the surface layer. What is interesting about this image is that there are dark and light horizontal stripes that represent, at a higher level of magnification, the fiber-like structures seen in Fig. 3(d). While we have no unambiguous evidence about the composition of the dark and light regions, we are tempted to interpret this brightness variation in terms of the presence of elongated domains of EB in the iPP matrix. The lamellar spacing appears

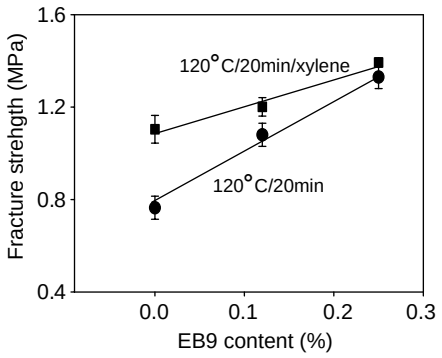

Fig. 4. Lap-shear strength of PP/CPO/PP, TPO_{12}/CPO/TPO_{12} and TPO_{25}/CPO/TPO_{25} samples plotted against EB content. The filled squares refers to samples that were exposed to hot xylene vapor (120 °C/20 min) prior to sandwich sample formation. The filled circles correspond to samples annealed at 120 °C/20 min without exposure to xylene vapor.

to be identical in both domains. This pattern resembles that seen in the inset of Fig. 4(a) reported by Chaffin et al. [18] in their study of blends of iPP with metallocene polyethylene polymers which they interpreted in terms of interfacial connectivity of the crystalline domains of both polymers. These authors attribute the enhanced strength of bond between the two components to the absence of non-crystallizable material in the metallocene ethylene copolymer coupled with the formation of entanglements at the iPP/mPE interface. A reviewer of our paper has pointed out that the thickness of the lamellar domains in Fig. 2(e) (ca. 6–9 nm) is in agreement with what one would expect from the melting temperature of iPP (165.2 °C) using the Gibbs–Thompson equation [19].

3.1. Composition dependence of the lap-shear strength

To compare the fracture strength development at the CPO/iPP or CPO/TPO interface, the lap-shear strength for two compositions of TPO and for pure iPP were measured. For these experiments, the CPO-coated iPP or TPO samples were annealed at 120 °C for 20 min to promote CPO chain diffusion into the iPP or TPO substrate. We found that the fracture strength increased with the EB content in TPO blends as shown in Fig. 4. The circles represent the samples that were not exposed to xylene vapor. The weakest adhesion is obtained with the iPP/CPO/iPP sample. Taking this as a baseline, we found that the fracture strength of the TPO_{12}/CPO/TPO_{12} and TPO_{25}/CPO/TPO_{25} sandwich samples increased by about 40 and 80%, respectively. Here TPO_{12} refers to a iPP/EB9 blend with a weight composition of 88/12, and TPO_{25} refers to a iPP/EB9 blend with a 75/25 wt% composition. The increase in fracture strength of the TPO/CPO/TPO samples is due to the presence of the EB9 rubber in the TPO blends.

The influence of the solvent exposure on the fracture strength of the iPP/CPO/iPP sandwich samples is also shown in Fig. 4. The square data points represent the samples that were exposed to xylene vapor during the thermal treatment. The fracture strength of iPP/CPO/iPP sandwich increased up to 40% compared to the samples without exposure to the xylene

vapor. The fracture strength of TPO/CPO/TPO samples also increased when the CPO/substrate bilayer samples were exposed to xylene vapor before fabricating the lap-shear sandwich samples. In the following sections, where we describe SEM and LCFM images of the fracture surface, it will be convenient to speak of 'polymer sandwich samples that were exposed to xylene vapor' We remind the reader that, in each instance, it was the CPO-coated substrate that was exposed to xylene vapor at 120 °C prior to fabrication of the lap-shear sandwich samples. We never actually exposed the three-layer sandwich samples to solvent vapors. Indeed, the xylene had evaporated from the CPO-coated substrates before the sandwich samples were assembled.

3.2. Fracture surface morphology probed by SEM and LCFM

Fig. 5 shows SEM images of the fracture surface of two iPP/CPO/iPP samples after lap-shear tests at room temperature. The image in the Fig. 5(a) is from a sample, which was not exposed to xylene vapor. This fracture surface was very smooth. The image in the Fig. 5(b) is for an identical polymer sandwich that was exposed to xylene vapor for 20 min at 120 °C. The fracture surface of this sample shows much more texture. In both samples, the failure occurred at the interface between CPO and iPP due to the weak interaction of the CPO and iPP components.

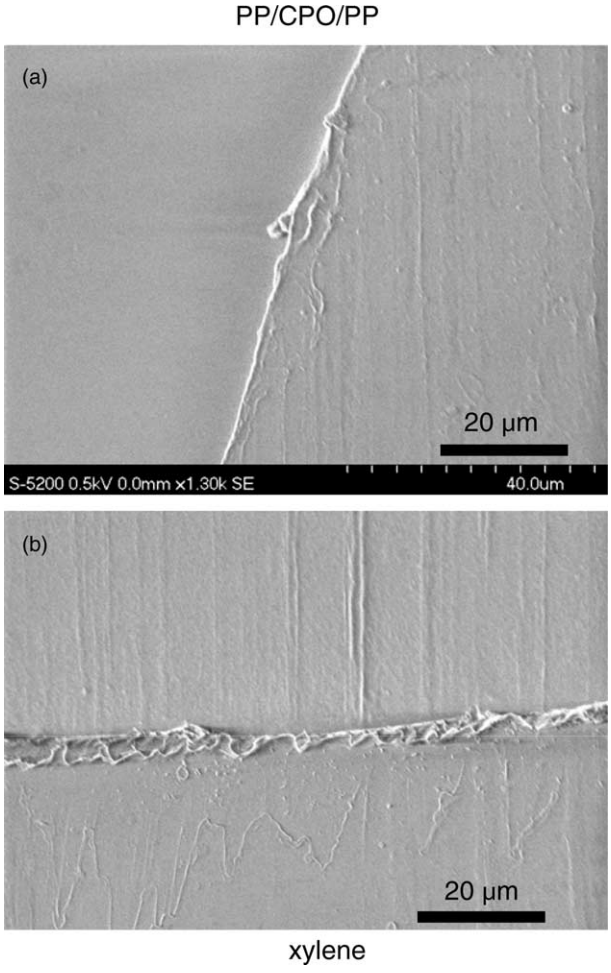

Fig. 5. SEM images of the PP/CPO/PP sandwich fracture surface of samples (a) annealed dry at 120 °C/20 min and (b) annealed at 120 °C/20 min in the presence of xylene vapor prior to sandwich sample formation.

Corresponding LCFM images of the fracture surface morphology of iPP/CPO/iPP sandwich samples are shown in Fig. 6. The white arrow in each image indicates the stress direction in the lap-shear facture experiment. Bright areas in the images correspond to the CPO layer, which contains the covalently bound fluorescent dye. In Fig. 6(a) and (b), one can see that the CPO layer was delaminated from the iPP substrate

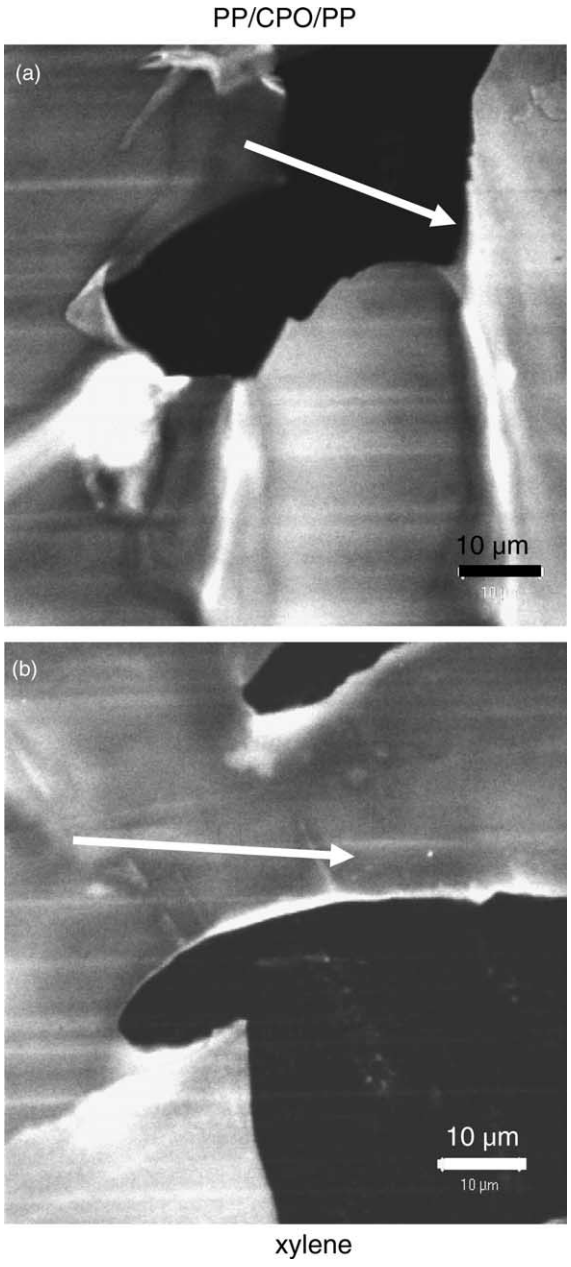

Fig. 6. Top view LCFM images of the PP/CPO/PP fracture surface of samples prepared without (a) and with exposure to xylene vapor (b). The size of each image window is 73×73 μm. The bright regions correspond to dye-labeled CPO, and the dark areas, to PP. The arrow in the image indicates the fracture direction during the lap-shear experiment.

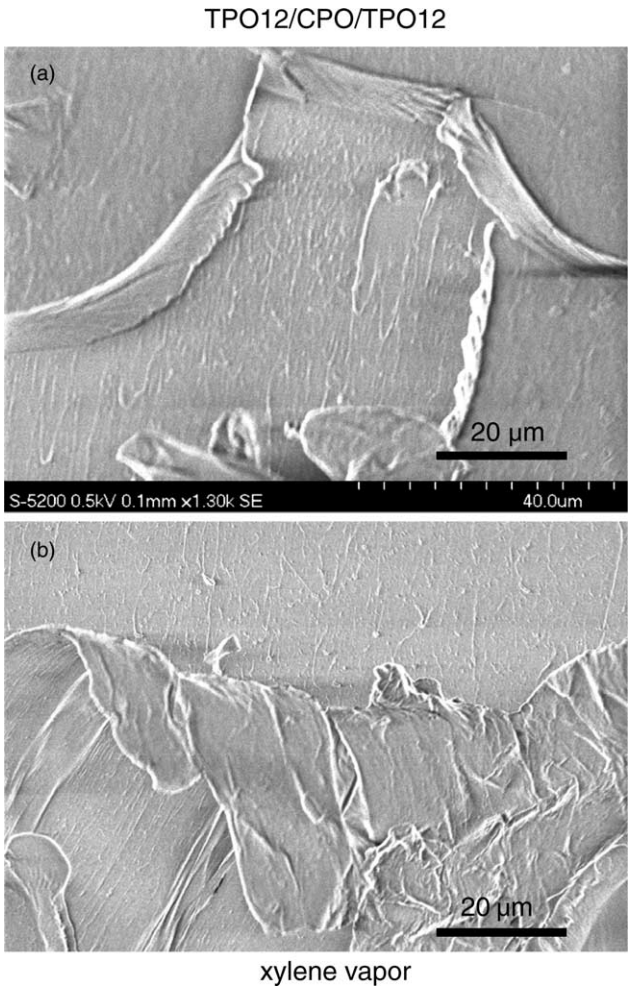

Fig. 7. SEM images of the TPO_{12}/CPO/TPO_{12} sandwich fracture surface of samples (a) annealed dry at 120 °C/20 min and (b) annealed at 120 °C/20 min in the presence of xylene vapor prior to sandwich sample formation.

surface irrespective of whether the samples were exposed to xylene vapor. Pieces of the CPO coating adhere loosely to each iPP surface, as can be seen in bright areas that appear in Fig. 6. The underlying iPP surface morphology appears to be relatively smooth in both samples, which is consistent with what one can perceive in the SEM images in Fig. 5(a) and (b). These results are consistent with relatively poor adhesion between CPO and iPP.

Fig. 7 shows SEM images of the fracture surface of two TPO_{12}/CPO/TPO_{12} samples after the lap-shear test following two different sample history conditions. The image in Fig. 7(a) is taken from a sample annealed dry at 120 °C for 20 min. On the upper left and on the right-hand side of the image, one sees what appears to be the TPO_{12} surface, with a thin film of a different material, presumably CPO, partially folded over in the center. The flat surface shows more texture than the corresponding iPP surface in Fig. 5(a). One obtains a similar result for the sample exposed to xylene vapor before lap-shear sample fabrication. In the image in Fig. 7(b), one sees a thin film that has been partially detached from the surface and has folded back upon itself during the lap-shear test. At the top of the image is a flatter surface, which shows a texture similar to that seen in Fig. 7(a).

LCFM images of these faces of the fracture surface show a bright fluorescence (white areas in Fig. 8(a) and (b)), which indicate that a significant amount of CPO has adhered to the TPO_{12} side of the facture surface. The dark lines in the image, which are aligned in the fracture direction in Fig. 8(a), indicate the presence of exposed regions of the TPO_{12} surface. While it is difficult to attribute all features of this image unambiguously, the darker vertical lines may indicate that some of the TPO component may have been pulled out of the substrate and folded over onto the CPO residue, creating shadows. The fracture surface of the xylene-treated sample seen in Fig. 8(b) shows a rougher texture, with substantial amounts of CPO

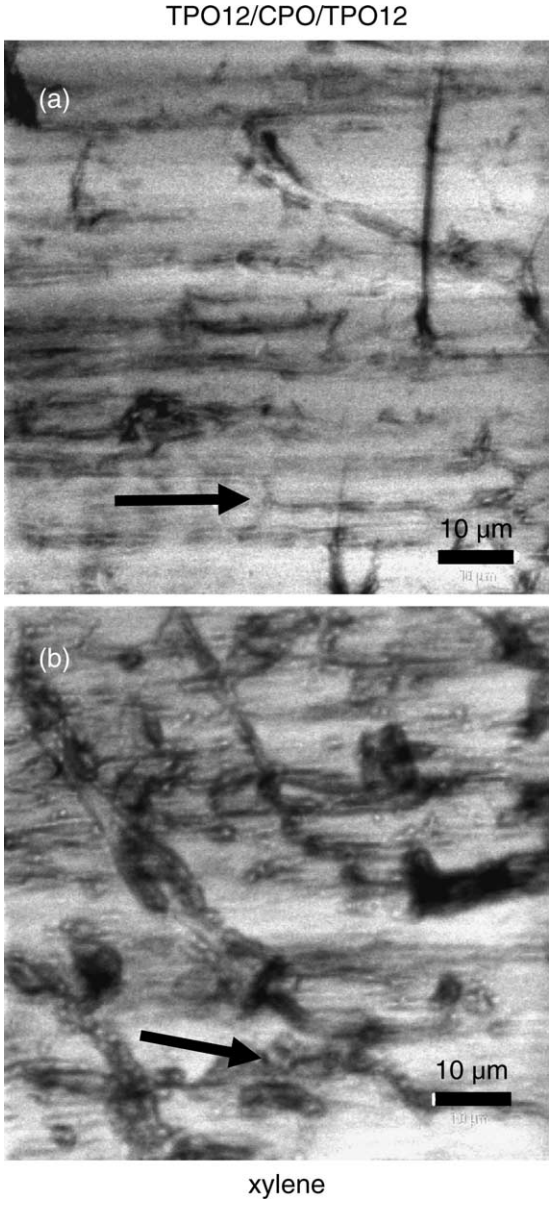

Fig. 8. Top view LCFM images of TPO_{12}/CPO/TPO_{12} fracture surface of samples prepared without (a) and with exposure to xylene vapor (b). The size of each image window is 73×73 μm. The arrow in the image indicates the fracture direction during the lap-shear experiment.

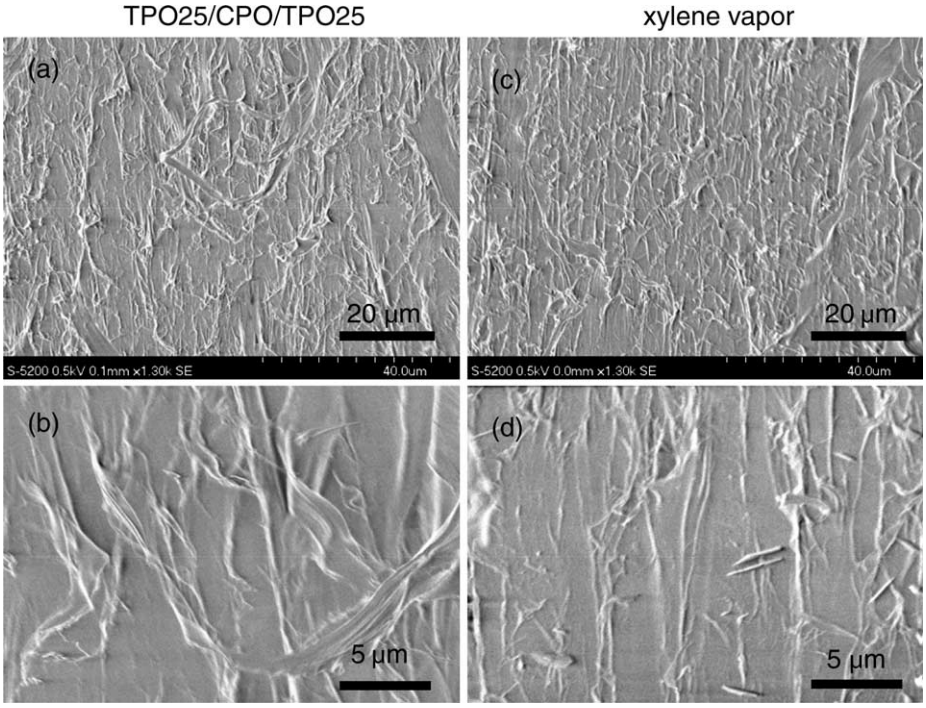

Fig. 9. SEM images of the TPO_{25}/CPO/TPO_{25} sandwich fracture surface of samples (a) and (b) annealed dry at 120 °C/20 min and (c) and (d) annealed at 120 °C/20 min in the presence of xylene vapor prior to sandwich sample formation. Images (b) and (d) represent a higher level of magnification as indicated by the scale bars.

adhering to the TPO_{12} side of the fracture surface, and with shadows that we suggest arise from pullout of TPO components during interfacial fracture. The rough texture of the fracture surface along with the presence of a CPO adhering to the TPO surface indicates that the interaction between CPO and TPO_{12} is stronger than that between CPO and iPP. Some non-fluorescent fibers can be seen as shadows on the top of the CPO layer.

SEM images of the fracture surface of TPO_{25}/CPO/TPO_{25} samples after the lap-shear test for two different baking conditions are shown in Fig. 9. The image in Fig. 9(a) is from the sample annealed dry at 120 °C for 20 min. This fracture surface is much rougher than that found in the corresponding TPO_{12} sample seen in Fig. 7(a). A strip-like morphology can be seen on the fracture surface. This roughened fracture morphology is associated with the higher fracture strength found in Fig. 4 for the samples not exposed to xylene vapor. Fig. 9(c) shows an SEM image of a corresponding TPO_{25}/CPO/TPO_{25} sample that had been exposed to xylene vapor. As in Fig. 9(a), one also observes a rough fracture surface. The similar texture of the fracture surface for these two TPO_{25}/CPO/TPO_{25} samples with different histories is consistent with the similar fracture energy for the two types of samples.

Higher magnification images of the samples seen in Fig. 9(a) and (c) are shown, respectively, in Fig. 9(b) and (d). The differences in the texture of the surface morphology are small, but we note that the fracture surface of the sample not exposed to xylene (Fig. 9(b)) shows a larger strip-like morphology of a film pulled away from, and then collapsed on, the surface of the sample after the lap-shear experiment. In contrast, Fig. 9(d) exhibits a thinner strip-like ruptured surface morphology.

Fig. 10(a) and (c) show top view LCFM images of the fracture surface of TPO_{25}/CPO/TPO_{25} samples after lap-shear tests at room temperature. The fracture surface of the TPO_{25}/CPO/TPO_{25} sample annealed without exposure to xylene is very rough. One can see that fracture has exposed regions of TPO_{25} (the dark areas in the image), but left large patches of CPO firmly attached. The roughness seen in this LCFM image corresponds to that seen by SEM in Fig. 9(a), but the LCFM image provides information about the chemical composition of the fracture surface. By SEM we saw little difference in the fracture surfaces of the samples prepared with and without exposure to xylene vapor. By LCFM, Fig. 10(c), we see a finer morphology in the xylene-treated sample. The CPO component appears in the form of relatively thin fibers stretched in the pull direction, and the image consists of parallel fluorescent and non-fluorescent bands. This fiber-like morphology can be found on both sides of the fracture surface of the TPO_{25} substrates, a result that indicates that the failure occurred near the CPO/substrate interface, but with significant adhesion of components from both sides of the interface.

We can get further information from side-view *xz*-scan sections of these fractured samples. These cross sections shown in Fig. 10(b) and (d) can be compared to those of the as-prepared and the annealed samples shown in Fig. 2. As one expects from the 5 μm thick CPO layer on each substrate, the CPO layer in the sandwich assembly is about 10 μm thick, and the fracture propagated near to one of the substrate surfaces. The bright grey CPO layer exhibits roughness at the top surface

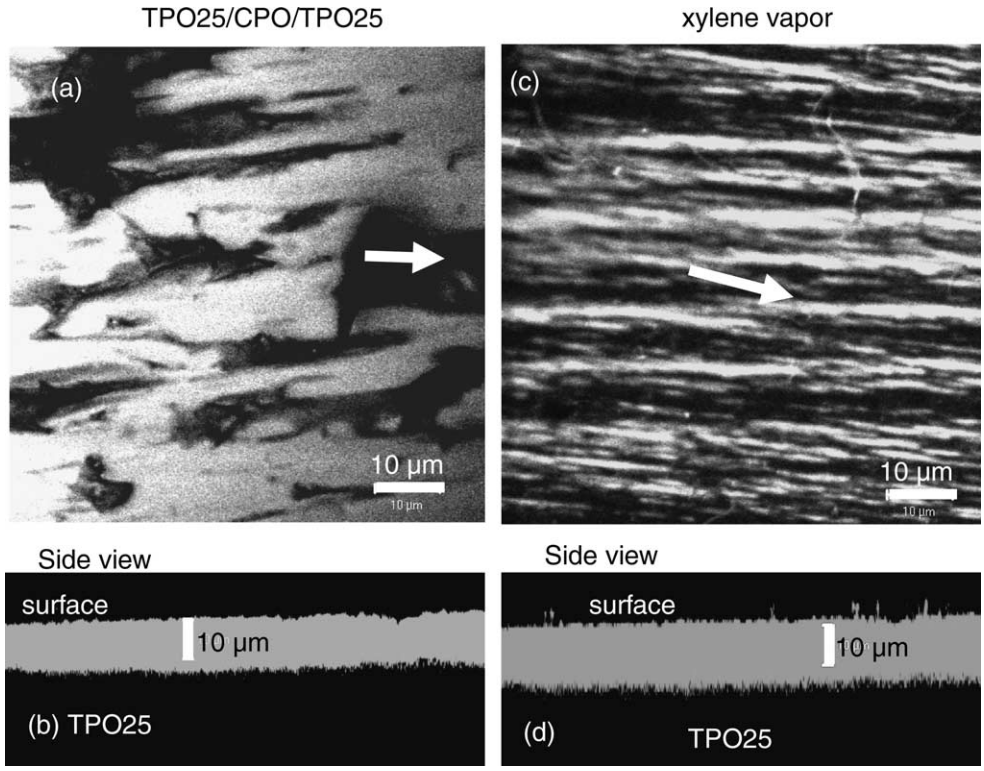

Fig. 10. Top view and side view LCFM images of the TPO_{25}/CPO/TPO_{25} fracture surface of samples (a) and (b) annealed dry at 120 °C/20 min and (c) and (d) annealed at 120 °C/20 min in the presence of xylene vapor prior to sandwich sample formation. (a) and (c) Top view images; (b) and (d) side view (*z*-scan) images. The white arrow in the top-view images indicates the fracture direction during the lap-shear experiment. The bright areas are due to dye-labeled CPO.

of the CPO layer, as well as thickness variations on a much longer length scale. The fact that the CPO layer, at these positions of the fracture, is significantly thicker than 10 μm, indicates that the CPO layer itself was partially deformed during the lap-joint test.

3.3. Lap shear tests on asymmetric samples

Further insights into the failure mechanism of the adhesion of CPO with TPO components are possible through lap-shear experiments on asymmetric samples. These samples were prepared in the same manner as those employed above, i.e. CPO-coated substrates were annealed dry, but the samples joined to make a three-layer sandwich sample consisted of two different polyolefin substrates. For example in iPP/CPO/TPO_{12} and iPP/CPO/TPO_{25}, the 10 μm thick CPO layer was in contact with iPP at one face and with TPO at the other face. When these samples were subjected to a lap-shear test, they tended to fracture near or at the interface with the substrate (e.g. iPP) with the weaker adhesion.

Fig. 11(a) shows a top view of the iPP face of the iPP/CPO/TPO_{12} sample after a lap-shear test at room temperature. In the image of the iPP face, one sees a dark background (iPP) with a few thin lines of fluorescent CPO adhering to the iPP. These fibers are aligned in the lap-shear direction indicated by the arrow in Fig. 11(a). The inset in this figure, which appears as a featureless light gray square, is a top view of the TPO face. There are few if any dark traces that would indicate places where iPP adhered to the CPO. A *z*-section cross section image of the TPO side of the same sample is shown in Fig. 11(b). This sample had not been exposed to xylene vapor. It is obvious from these images that fracture occurred at the iPP/CPO interface and that the CPO layer is almost exactly 10 μm thick. The fracture surface is flat and relatively sharp.

Corresponding images for the fracture surface of a iPP/CPO/TPO_{25} sample after a lap-shear test are shown in Fig. 11(c) and (d). The iPP face shows a large number of places where a small amount of CPO remains in contact with the iPP surface. These areas are also elongated in the direction of the shear. The inset, showing the TPO_{25} face, is uniformly bright, again indicating no tendency for the fracture to leave iPP in contact with the CPO layer. The fracture surface seen in cross-section in Fig. 10(d) is also flat and relatively sharp. One can also see that the CPO layer in this sample and in Fig. 10(b) is uniform and not distorted and is almost exactly 10 μm thick.

Fig. 12 shows the top view and side view (TPO_{25} part) LCFM images of the fracture surface morphology of a TPO_{12}/CPO/TPO_{25} sandwich sample after a lap-shear test at room temperature. From the *xz*-scan image in Fig. 12(c), one can see that fracture occurred exclusively at the CPO/TPO_{12} interface. The dark area at the top of this image is the air surface where the TPO_{12} layer had been attached. One can see that this fracture surface is relatively smooth, with sites in which chunks of the CPO were pulled from the CPO layer during fracture. Deformation of the CPO layer has led to a layer thickness significantly larger than 10 μm.

In Fig. 12(a), we present a top-view image of the TPO_{12} face of the fracture surface. It is largely dark, indicating that

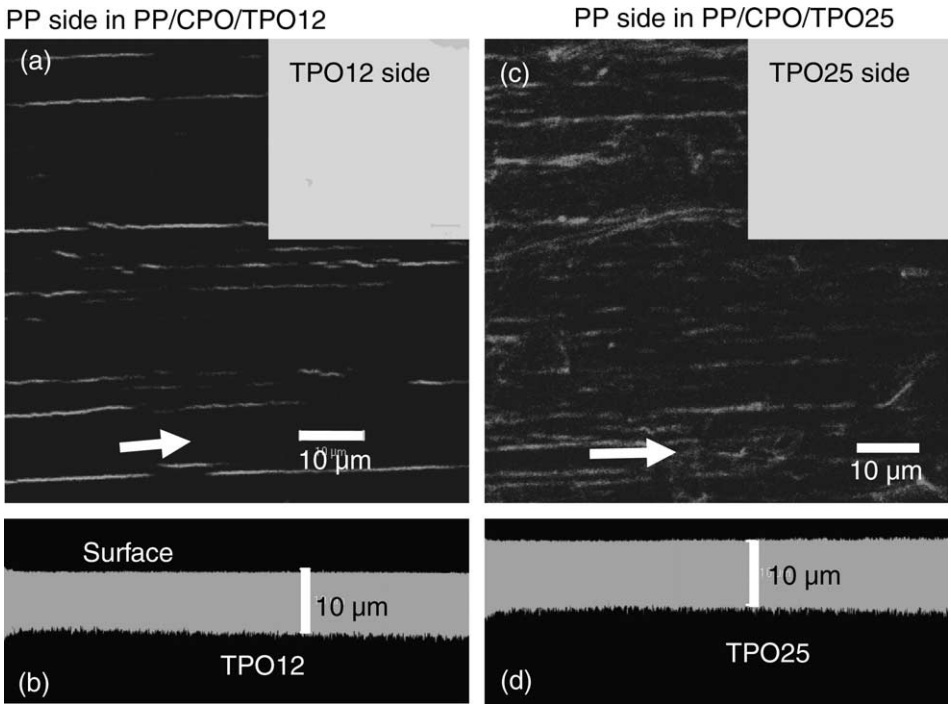

Fig. 11. Top (a) and (c) and side (b) and (d) view LCFM images of the PP/CPO/TPO_{12} and PP/CPO/TPO_{25} fracture surfaces. (a) Top view image of the PP side (the insert is the corresponding (featureless) image of the TPO_{12} side) of the PP/CPO/TPO_{12} fractured sample. (b) Side view LCFM image of the TPO_{12} part of this sample. (c) Top view image of the PP side (the insert is the corresponding (featureless) image of the TPO_{25} side) of the PP/CPO/TPO_{25} fractured sample. (d) Side view LCFM image of the TPO_{25} part of this sample. The white arrow in the top-view images indicates the fracture direction during the lap-shear experiment.

relatively little CPO adhered to this face. There are bright patches on this surface due to residual CPO, and they are strongly elongated in the fracture direction. A top-view image of the TPO_{25} part is shown in Fig. 12(b). Here the surface is largely bright because one is looking at a CPO-coated substrate, but dark patches can be seen. The dark patches are holes in the CPO layer indicating regions of the sample where the fracture passed through the CPO phase and left portions of the TPO_{25} substrate surface exposed. The brightest areas in this image are exposed regions of dye-labeled CPO. The darker (here grayer) surface represents shadowing caused by TPO_{12} from the top surface that remains in contact with the fracture surface of the sample. This part of the surface is reminiscent of that seen in Fig. 8(a). Taken together, these images indicate stronger adhesion between TPO_{25} and CPO than for TPO_{12} and CPO. Fracture propagates close to the interface between CPO and the weaker adhering substrate. The adhesion difference is small enough that the fracture surface occasionally passed from one face of the CPO layer to the other. It is clear that the adhesion between CPO and TPO is much stronger than that between CPO and iPP itself.

4. Summary and conclusions

We described experiments that examine the failure mechanism of a CPO coating on a high-modulus TPO fabricated as a blend of a highly crystalline Ziegler-Natta polypropylene and a crystalline metallocene poly(ethylene–butene) (EB9) impact modifier. The CPO itself had relatively low chlorine content (20 wt%). The CPO was doped with a small amount (5%) of a similar CPO to which a fluorescent dye was covalently attached.

Injection-molded samples of iPP+EBR9 blends gave a different surface morphology than that described for TPO samples based upon ethylene–propylene rubber. We find a well-defined skin layer approximately 230 μm thick at the mold surface. For the 25 wt% EB9 blend, this skin layer consists of thin fibers of EB trapped in transcrystalline iPP matrix. We observe an identical lamellar spacing in both domains. This type of pattern for polypropylene blends with metallocene polyethylene was first described by Chaffin et al. [18] and move recently examined by Hiltner et al. [20].

Lap-shear fracture tests of iPP/CPO/iPP sandwich samples show that exposure of CPO coated iPP to vapors of xylene during the bake cycle leads to a 40% increase in fracture strength compared to the samples baked dry. In spite of the enhanced adhesion, few differences were observed in the facture surface itself observed by SEM or LCFM.

For example, the fracture propagated adjacent to the CPO/iPP interface, and the CPO layer after fracture maintained its original thickness (ca. 10 μm) with no sign of distortion. The most surprising observation was the finding of a thin film of CPO partially debonded from the iPP surface, which indicates that the fracture propagates in part through the CPO in the near-surface region. The plastic deformation of this layer may be responsible for much of the energy dissipated on debonding. The dramatic increase in the fracture strength for the solvent-exposed sample may be due to the disturbance of the

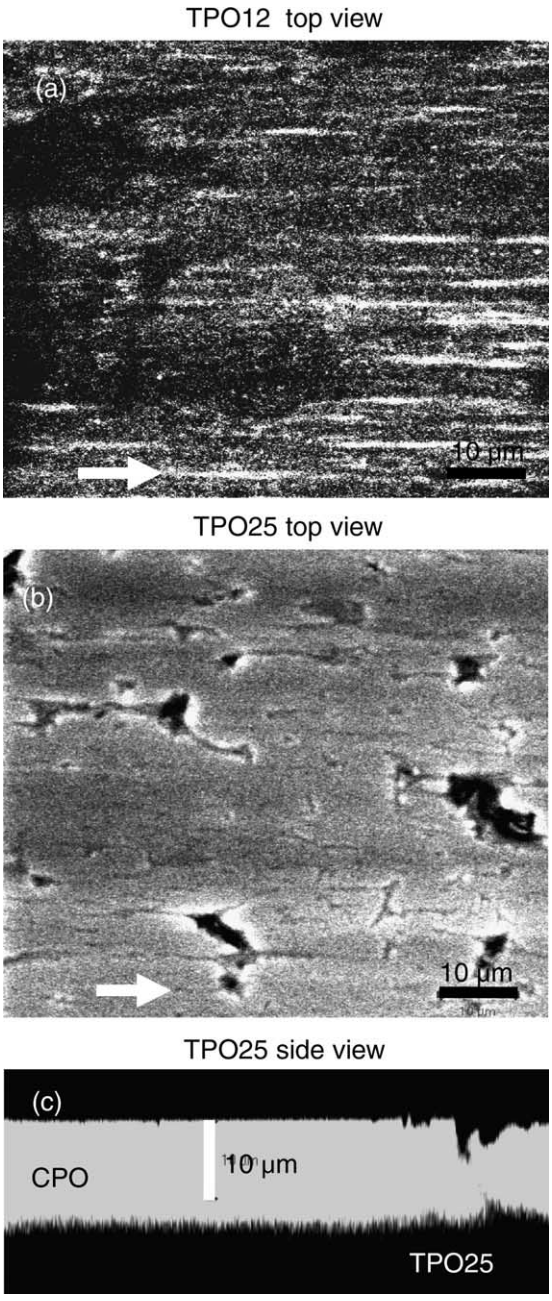

Fig. 12. Top view and side view LCFM images of the TPO_{12}/CPO/TPO_{25} fracture surface; (a) Top view image of the TPO_{12} side; (b) top view image of the TPO_{25} side and (c) side view (z-scan) image of the TPO_{25} part of the fractured sample. The arrow in the image indicates the fracture direction during lap-shear experiment.

crystal structure of iPP near the surface region in the presence of the solvent vapors accompanied by interpenetration of CPO and iPP polymer chains.

Our observation that the lap-shear fracture strength for CPO/polyolefin increased with higher EB9 content is consistent with many previous reports of CPO adhesion to other TPO compositions [8]. This effect is particularly prominent for the samples that were annealed dry. It is important to note that EB9 is a semicrystalline impact modifier, and that iPP has a higher degree of the crystallinity (43.4%) than EB9 (29%). The 120 °C bake temperature used in these experiments is higher than the melting temperature (T_m) of EB9 and lower than that of the iPP. One of the surprises of our results is that the xylene-vapor treatment has such a large effect on enhancing the strength of adhesion of CPO to the high modulus iPP. As one can see in Fig. 4 the Lap-shear strength of this sample is within one standard deviation of that for the xylene-vapor treated TPO_{12} sample and not very much smaller than that for TPO_{25}.

The influence of xylene on the strength of adhesion of this CPO to TPO_{12} and CPO_{25} is much smaller. For the specific example of TPO25, the xylene-vapor treated sample and the dry-baked sample had the same fracture strength within experimental error. This is a useful result from the perspective of removing aromatic hydrocarbons from automotive coatings and replacing them with more polar oxygenated solvents to meet the upcoming hazardous air pollutant substance (HAPS) regulations. While this type of solvent replacement would likely reduce the fracture strength of the iPP/CPO/iPP system, it would have little effect on the TPO_{25}/CPO/TPO_{25} system.

The fracture surface morphology provides information on the mechanism or the weak point of failure. For both the symmetric iPP/CPO/iPP and the asymmetric iPP/CPO/TPO sandwich samples, the LCFM images indicate that failure occurred close to the interface between the CPO and the iPP substrate, and the CPO layer maintained its original thickness. For the TPO_{12}/CPO/TPO_{12} and TPO_{25}/CPO/TPO_{25} sandwich samples, the fracture surfaces themselves were much rougher than that between CPO and iPP, and indicated much better adhesion between the CPO and TPO components. While failure occurred in the region of the TPO/CPO interface, there were indications of ductile deformation of regions of the TPO surface, and the CPO layer itself was deformed. Failure was due primarily to the cohesive fracture of the CPO in the region adjacent to the TPO substrate.

Acknowledgements

The authors would like to thank Visteon, E.I. Dupont Canada, and NSERC Canada for financial support of this research. We also thank Nippon Paper Ind. Ltd for kindly providing the CPO sample used in this study.

References

[1] Garbassi F, Morra M, Occhiello E, editors. Polymer surfaces: from physics to technology. New York: Wiley; 1994 [chapter 10].
[2] Prater TJ, Kaberline SL, Holubka JW, Ryntz RA. J Coat Technol 1996; 68(857):83–91.
[3] Ryntz RA, Xie Q, Ramamurthy AC. J Coat Technol 1995;67(843):45–55.
[4] Ryntz RA, Ramamurthy AC. J Coat Technol 1995;67(840):35–46.
[5] Morris HR, Munroe B, Ryntz RA, Treado PJ. Langmuir 1998;14: 2426–34.
[6] Mirabella FM, Dioh N, Zimba CG. Polym Eng Sci 2000;40:2000–6.
[7] Tang H, Martin DC. J Mater Sci 2002;37:4777–85.
[8] Tomasetti E, Legras R, Henri-Mazeaud, Nysten B. Polymer 2000;41: 6597–602.
[9] Ellis TS. Polym Eng Sci 2001;41:2065–72.

[10] Ma Y, Farinha JPS, Winnik MA, Yaneff P, Ryntz RA. Macromolecules 2004;37(17):6544–52.
[11] Boivin KC, Barry CMF, Orroth SA. SPE ANTEC'99 1999;3:3157–61.
[12] Brandrup J, Immergut H, editors. Polymer handbook. 3rd ed. New York: Wiley; 1989.
[13] Fijiyama M, Wakino T. J Appl Poly Sci 1991;43:57–81.
[14] Kornfield JA, Kumaraswamy G, Issaian AM. Ind Eng Chem Res 2002;41: 6383–92.
[15] Ryntz RA. J. Vinyl Addit Technol 1997;3(4):295–300.
[16] Moffitt M, Rharbi Y, Chen W, Tong J, Winnik MA, Thurman DW, et al. J Polym Sci, Part B: Polym Phys 2002;40:2842–59.
[17] Ryntz RA. Prog Org Coat 1996;27:241–54.
[18] Chaffin KA, Bates FS, Brany P, Brown GM. J Polym Sci, Part B: Polym. Phys. 2000;38:108–21.
[19] see Keller A. In: Dosière M, editor. Crystallization of polymers. NATO ASI series C: mathematical and physical sciences, vol. 405. Dordrecht, The Netherlands: Kluwer; 1993. p. 5.
[20] Poon BC, Chum SP, Hiltner A, Baer E. Polymer 2004;45:893–903.